Effects of shear flow on a polymeric bicontinuous microemulsion: Equilibrium and steady state behavior

Kasiraman Krishnan, Bryan Chapman,[a] Frank S. Bates,[b),c)]

and Timothy P. Lodge[b),d)]

Department of Chemical Engineering and Materials Science, University of Minnesota, Minneapolis, Minnesota 55455

Kristoffer Almdal

Risø National Laboratory, DK-4000 Roskilde, Denmark

Wesley R. Burghardt

Department of Chemical Engineering, Northwestern University, Evanston, Illinois 60208

(Received 13 August 2001; final revision received 27 November 2001)

Synopsis

We have investigated the effects of shear flow on a polymeric bicontinuous microemulsion using neutron scattering, light scattering, optical microscopy, and rheology. The microemulsion consists of a ternary blend of poly(ethyl ethylene) (PEE), poly(dimethyl siloxane) (PDMS), and a PEE–PDMS diblock copolymer. At equilibrium, the microemulsion contains two percolating microphases, one PEE rich and the other PDMS rich, separated by a copolymer-laden interface; the characteristic length scale of this structure is 80 nm. Low strain amplitude oscillatory shear measurements reveal behavior similar to that of block copolymer lamellar phases just above the order–disorder transition. Steady shear experiments expose four distinct regimes of response as a function of the shear rate. At low shear rates (regime I) Newtonian behavior is observed, whereas at intermediate shear rates (regime II) development of anisotropy in the morphology leads to shear thinning. When the shear rate is further increased, there is an abrupt breakdown of the bicontinuous structure, resulting in flow-induced phase separation (regime III). Rheological measurements indicate that the shear stress is almost independent of the shear rate in this regime. Light scattering reveals a streak-like pattern, and correspondingly a string-like morphology with micron dimensions is observed with video microscopy. Upon a further increase of the shear rate (regime IV), the sample resembles an immiscible binary polymer blend with the block copolymer playing no significant role; the stress increases strongly with the shear rate. In some respects these results resemble those from other weakly structured complex fluids (sponge phases, liquid crystals, worm-like micelles,

[a)]Current address: ExxonMobil Chemical Co., Baytown Polymers Center, Baytown, TX 77520.
[b)]Authors to whom all correspondence should be addressed.
[c)]Electronic mail: bates@cems.umn.edu
[d)]Also at Department of Chemistry, University of Minnesota, Minneapolis, MN 55455.

block copolymers, polymer blends, and polymer solutions), yet in important ways this system is unique. [DOI: 10.1122/1.1446883]

I. INTRODUCTION

Complex fluids including polymer solutions and blends, surfactants, liquid crystals, block copolymers, and colloids often exhibit fascinating rheological properties, and can undergo a variety of morphological transformations under flow. The complex internal microstructure of these fluids leads to behavior that is vastly different from that of conventional Newtonian or non-Newtonian fluids. In many cases shear flow is found to disrupt the equilibrium morphology and to induce apparent shifts in phase boundaries.

Bicontinuous microemulsions, formed by mixing appropriate amounts of oil, water, and a surfactant [Scriven (1976)] form an intriguing class of complex fluids. They possess a characteristic nanostructure consisting of undulating surfaces with vanishingly small interfacial curvature. Other properties of these fluids include a very large amount of interfacial area and negligible surface tension due to the presence of the amphiphile. With their complicated and delicately balanced internal structure, one can expect bicontinuous microemulsions to exhibit rich rheological properties. However, there have been relatively few reports of the rheological behavior of oil–water–surfactant (o/w/s) bicontinuous microemulsions [Chen and Warr (1992); Anklam *et al.* (1995); Warr (1995)]; such studies have been hindered by rapid microstructural dynamics, which necessitate the use of extremely high shear rates.

Recently we have demonstrated the utility of ternary polymer blends as model surfactant systems [Washburn *et al.* (2000)]. In particular, bicontinuous microemulsions can be generated in polymers by mixing appropriate amounts of two homopolymers and the corresponding diblock copolymer [Bates *et al.* (1997); Fredrickson and Bates (1997); Hillmyer *et al.* (1999); Matsen (1999); Kielhorn and Muthukumar (1997)]. One expects the dynamics of polymeric bicontinuous microemulsions to be much slower than those of o/w/s bicontinuous microemulsions due to higher molecular weights and larger viscosities. Here we present a systematic experimental investigation of the dynamic response of a model polymeric bicontinuous microemulsion.

Flow-induced effects on soft materials have been described in numerous publications. Sponge phases consist of a three-dimensional network of a bilayer of surfactant molecules that separates the solvent into two subvolumes, and closely resemble bicontinuous microemulsions. Mahjoub *et al.* (1998) and Yamamoto and Tanaka (1996) have reported the shear-induced transition of the sponge phase to a lamellar state. Berret *et al.* (1994, 1998) have observed a shear-induced isotropic to nematic transition in worm-like micellar solutions. Warr (1995) and Anklam *et al.* (1995) described shear thinning in ternary o/w/s bicontinuous microemulsions at very high shear rates (10^3–10^4 s^{-1}). A shear-induced increase in the isotropic to lamellar transition temperature was predicted by Cates and Milner (1989), and documented in diblock copolymers by Koppi *et al.* (1993). In contrast, lamellae-forming triblock and pentablock copolymers exhibit shear-induced disordering [Tepe *et al.* (1997); Vigild *et al.* (2001)]. Shear alignment of block copolymer lamellae can result in parallel or perpendicular orientations, depending on the shear frequency and the temperature [Koppi *et al.* (1992); Fredrickson (1994); Gupta *et al.* (1995)]. Nakatani *et al.* (1997) investigated block copolymer-modified homopolymer blends and found that shear flow has a destabilizing effect on the disordered phase above a threshold block-copolymer concentration. Pätzold and Dawson (1996) made predictions of the rheological properties of a bicontinuous microemulsion using a Landau–Ginzburg model.

Flow effects on polymer solutions and blends also have attracted significant interest. Semidilute polymer solutions near the coexistence curve are found to exhibit enhanced concentration fluctuations or phase separation under shear flow [Menasveta and Hoagland (1991); Moses *et al.* (1994); Migler *et al.* (1996); Kume *et al.* (1997)]. A common feature of these studies is the appearance of so-called ''butterfly'' light scattering patterns. Flow in polymer blends often causes apparent shifts in phase boundaries [Hashimoto *et al.* (1988); Nakatani *et al.* (1990)], leading to either flow-induced mixing [Nakatani *et al.* (1990); Kim *et al.* (1997); Hindawi *et al.* (1992)] or demixing [Fernandez *et al.* (1995); Gerard *et al.* (1999); Chopra *et al.* (1998)]. Recently Martys and Douglas (2001) reported calculations for flow-induced phase separation in lattice-Boltzmann fluid mixtures. In most of these cases, phase-separated blends are found to exhibit a string-like morphology aligned along the flow direction.

The equilibrium phase behavior of a ternary polymeric system A/B/A–B can be represented in the form of a phase prism as shown in Fig. 1. Simpler phase diagrams can be obtained by cutting the prism with horizontal or vertical planes. The former gives an isothermal ternary phase diagram, while the latter yields a phase diagram at a constant ratio of the homopolymer concentrations. A schematic of the isothermal phase diagram is shown in Fig. 1(a) for the case of a symmetric copolymer and equal homopolymer molecular weights. Ordered morphologies including lamellae, hexagonally packed cylinders, and cubic (gyroid and spherical) phases are prevalent at high block copolymer concentrations [Washburn *et al.* (2000)], while macroscopic phase separation into two or three phases occurs at low diblock concentrations. The gray triangle in Fig. 1(a) represents the three-phase window, with coexistence between two homopolymer-rich phases and a middle bicontinuous microemulsion phase. This three-phase triangle is surrounded by two-phase regions, and the bicontinuous microemulsion ($b\mu E$) phase is present over a small composition range at the tip of this triangle.

The phase diagram along a vertical plane of the prism is an isopleth, and the example shown in Fig. 1(b) corresponds to nearly equal volume fractions of the homopolymers. The total homopolymer volume fraction is plotted along the abscissa and the temperature along the ordinate. At high temperatures, only a disordered phase exists, whereas at low temperatures, there are three regimes. At low homopolymer concentrations (i.e., high block copolymer concentrations), this symmetric mixture produces a lamellar phase. With only small amounts of the amphiphile (< 10 vol %), two-phase and three-phase regions occur as anticipated by Fig. 1(a). In between the lamellar and phase-separated regions, there is a narrow channel of bicontinuous microemulsion. Typically this corresponds to a block copolymer concentration of 8–12 vol % [Hillmyer *et al.* (1999)]. We have characterized this bicontinuous microemulsion phase for various polymeric systems in previous studies [Bates *et al.* (1997); Hillmyer *et al.* (1999); Morkved *et al.* (1999)], and recently we noted the intriguing rheological behavior of a polymeric bicontinuous microemulsion under shear [Krishnan *et al.* (2001)]. In this article we explore details of the rheological and structural properties under steady shear flow at different shear rates and temperatures that extend deep into the microemulsion channel.

II. EXPERIMENTS

A. Materials

The work described here was performed with a single ternary blend of poly(ethyl ethylene) (PEE), poly(dimethyl siloxane) (PDMS), and a PEE–PDMS diblock copolymer. These polymers were synthesized by standard anionic polymerization and catalytic saturation techniques that are described elsewhere [Hillmyer *et al.* (1999)]. PEE was

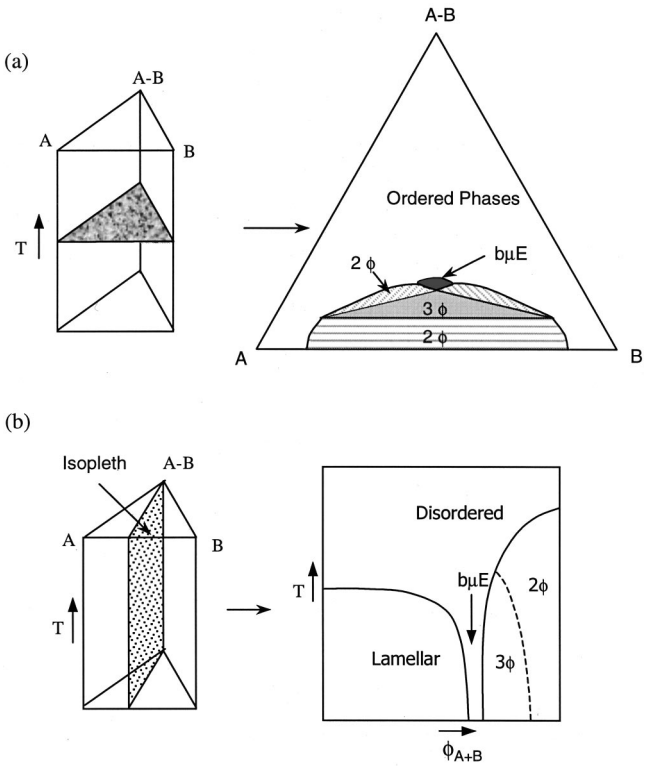

FIG. 1. Schematic phase diagram of ternary polymer blends A/B/A–B: (a) isothermal phase diagram; the hatched areas indicate two-phase regimes; the gray triangle represents the three windows at the tip of which the bicontinuous microemulsion region is located; (b) phase diagram along an isopleth (with equal amounts of homopolymers); the total homopolymer volume fraction is plotted along the abscissa.

prepared by saturating 1,2-polybutadiene with deuterium, in both the homopolymer and the diblock copolymer samples. Number average molecular weights, determined by nuclear magnetic resonance (NMR) spectroscopy, were 1770, 2130, and 10,400 for PEE, PDMS, and PEE-PDMS, respectively. The densities were measured using a density gradient column and the volume fraction of PEE in the block copolymer was determined to be 52%. This block copolymer molecular weight places the order–disorder transition temperature (90 °C) close to the critical temperature of the corresponding binary homopolymer blend (150 °C); an additional benefit afforded by these relatively low molecular weights is rapid phase transition dynamics, which facilitate equilibration. A single symmetric composition containing 10% by volume block copolymer and 45% PEE and PDMS homopolymers was used throughout this study. This mixture lies in the bicontinuous microemulsion channel which was identified in earlier publications [Hillmyer *et al.* (1999); Morkved *et al.* (1999)]. Specimens were prepared by simple mixing at 80 °C (in the disordered state) followed by cooling to room temperature.

B. Experimental techniques

Small angle neutron scattering (SANS) experiments were conducted at the National Institute of Standards and Technology (NIST), Gaithersburg, Maryland, on the 30 m NSF/CHRNS SANS instrument using $\lambda = 12$ Å wavelength neutrons ($\Delta\lambda/\lambda = 0.11$). A quartz couette shear cell was used, with the neutron beam directed radially through two sections of the device (Fig. 2). Additional SANS experiments were conducted with the

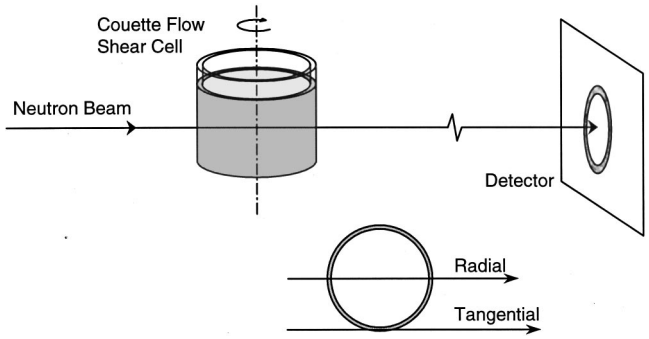

FIG. 2. Schematic diagram of the SANS experimental setup. The shear cell has Couette flow geometry with a rotating inner cylinder The beam was directed both in the radial and tangential directions.

neutron beam impinging tangentially. The Couette cell gap was 0.5 mm, leading to a total scattering thickness of 1 mm. Steady state patterns were collected at various temperatures and shear rates. The data were corrected for background and cell scattering, sample thickness, transmission, and detector sensitivity.

Small angle light scattering (SALS) experiments were carried out using a custom-built flow-light scattering apparatus, illustrated in Fig. 3. This instrument contains a shear stage (Linkam Scientific Instruments) that employs a rotating parallel plate geometry with transparent disks. The temperature can be controlled to a precision of $\pm 0.2\,^{\circ}\mathrm{C}$ using a silver heating block along with circulating cooling water in the body of the stage. A He–Ne laser ($\lambda = 632.8$ nm) supplies the light beam, which is conditioned by a set of neutral density filters, an iris, and a pair of alignment mirrors before passing through the sample. Two-dimensional scattering patterns are projected onto a translucent frosted glass screen, imaged by a charge coupled device (CCD) camera connected to a VCR, and recorded using high quality S-VHS videotapes. Subsequently these images were digitized from the videotapes using a computer equipped with frame-grabbing capabilities. Real-space microscopic images were obtained using the same shear stage mounted on an optical microscope (Olympus), with a long working-distance objective.

Rheological measurements were carried out with a strain-controlled Rheometric Scientific ARES rheometer. A cone and plate geometry with a 50 mm plate diameter and 0.02 rad cone angle was used. The sample was maintained under nitrogen atmosphere and the temperature was controlled to within $\pm 0.1\,^{\circ}\mathrm{C}$. Dynamic frequency sweep experiments were performed in the linear regime with frequencies from 0.01 to 100 rad/s. Steady shear rate sweep experiments were executed over the range from 0.01 to 250 s^{-1}. Transient shear flow startup experiments were conducted prior to the rate sweep in order to determine the time required to reach steady state at several representative shear rates. The sample was viewed at high magnification using a video camera to verify the absence of edge fracture at high rates. Rate sweeps were carried out with both increasing and decreasing rates, and no hysteresis effects were evident in the viscometric properties. These experiments were repeated at various temperatures over the range of $0–35\,^{\circ}\mathrm{C}$, while maintaining a constant cone-to-plate gap by taking into account thermal expansion of the tools.

III. RESULTS AND ANALYSIS

A. Rheology

Dynamic frequency sweep experiments were performed on the bicontinuous microemulsion sample at various temperatures. Stress relaxation experiments established a

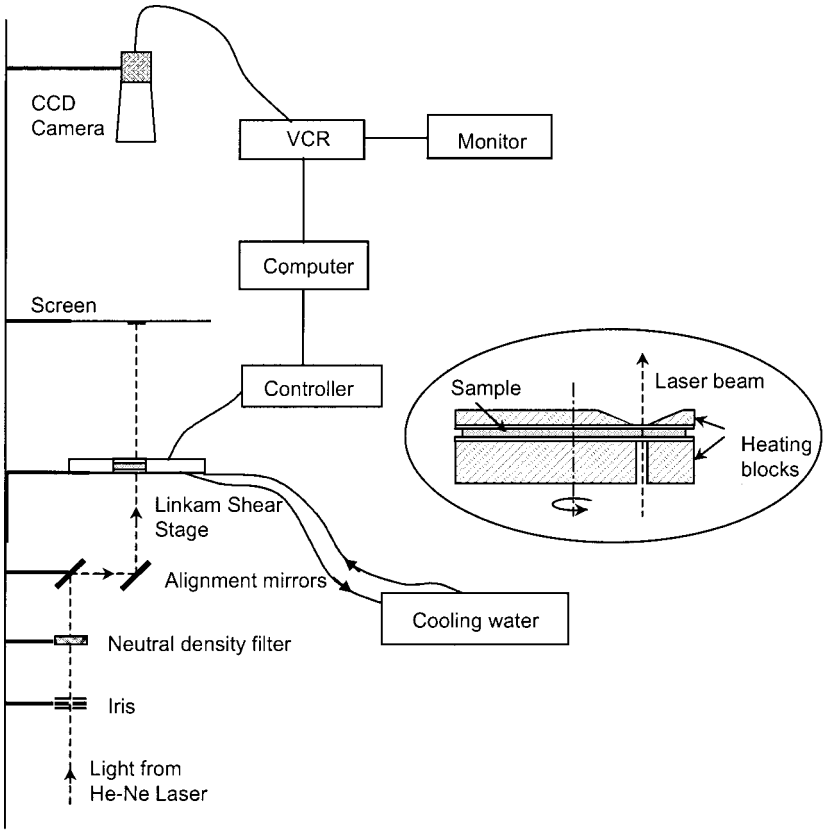

FIG. 3. Schematic diagram of the flow-light scattering experimental setup. The inset is a cross-sectional view of the shear cell.

linear viscoelastic response for strains less than 50%. Therefore, frequency sweep data were collected using 10% strain at lower temperatures and 20% strain at higher temperatures, well within the linear regime. Raw linear viscoelastic data obtained at various temperatures are presented in Fig. 4 as the magnitude $|\eta^*|$ and phase angle δ of the dynamic viscosity versus frequency ω. The complex viscosity exhibits a plateau at low frequencies followed by relaxation at high frequencies [Fig. 4(a)], behavior typical of a polymeric liquid. Closer inspection reveals, however, that the extent of the relaxation is more pronounced at low temperatures. As a result, these data cannot be reduced to a unique master curve by time–temperature superposition, a point reinforced by the phase angle plot [Fig. 4(b)]. Terminal, liquid-like behavior is evident at the lowest frequencies and highest temperatures (δ approaches 90°). A decreasing phase angle indicates an increasing elastic character in the viscoelastic response up to intermediate frequencies, after which the trend reverses towards a more viscous response at high frequencies. Shifts in the curves towards lower frequency at low temperatures reflect a slowing down of the dynamics. In addition, the minimum value of phase angle decreases at lower temperature, indicating that the mixture becomes more elastic at lower subcoolings within the microemulsion channel. Viscoelastic materials that obey time–temperature superposition allow simple shifting of the phase angle along the frequency axis; clearly the microemulsion is not thermorheologically simple.

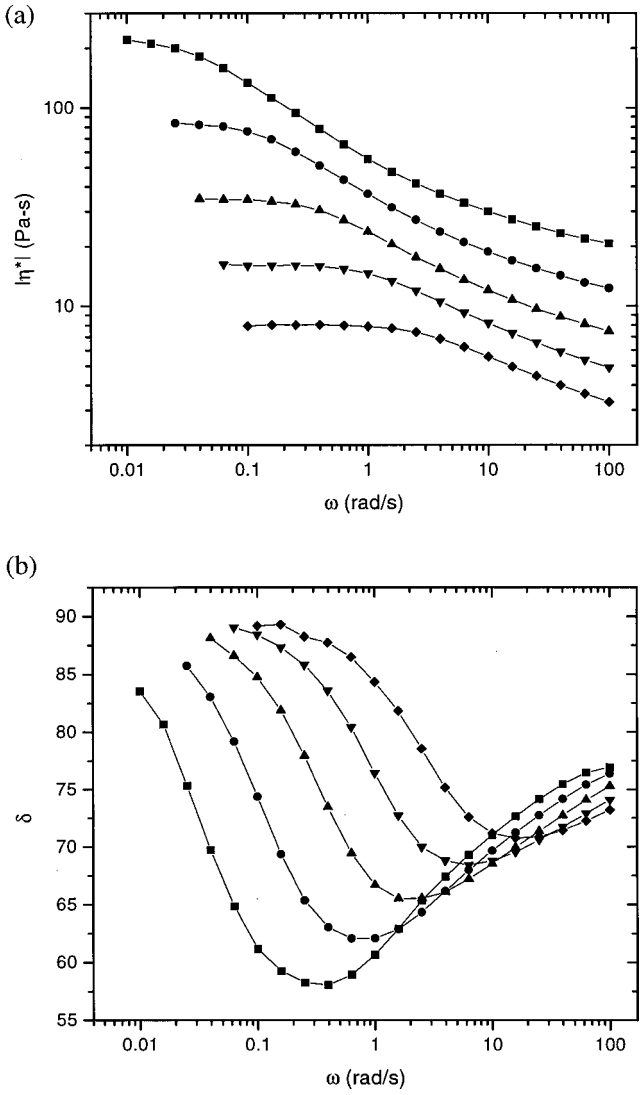

FIG. 4. Dynamic frequency sweep data on bicontinuous microemulsion at 10 (■), 15 (●), 20 (▲), 25 (▼), and 30 °C (♦): (a) zero-shear viscosity vs the frequency (ω) and (b) phase angle vs the frequency (ω).

Figure 5(a) presents a cross plot of G'' vs G' [Han *et al.* (1995)]. Data collected at different temperatures should collapse onto a single curve in such a plot for viscoelastic materials that obey time–temperature superposition. Here we see that the data converge at high values of G'' and G' (e.g., at high frequencies), whereas they fail to superimpose at low frequencies. We surmise that the low frequency response reflects the viscoelasticity associated with the microemulsion structure, which is temperature dependent. A decrease in temperature increases the degree of segregation between the constituents, leading to a larger viscoelastic contribution by the supermolecular structure. Conversely, the high frequency response presumably is dominated by more local-scale dynamics, which should be less affected by changes in the thermodynamic state of the microemulsion. These data suggest that the most meaningful way by which to shift the viscoelastic data along the frequency axis is to attempt to achieve superposition at high frequency; this is

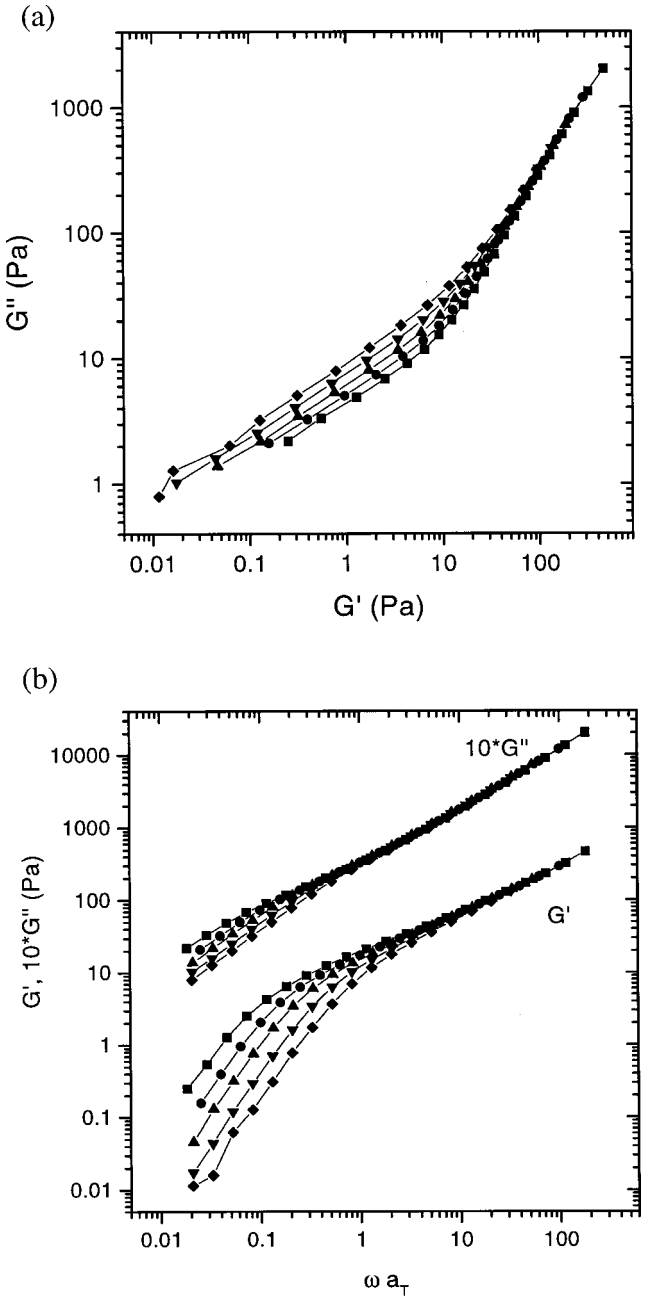

FIG. 5. Dynamic frequency sweep data on bicontinuous microemulsion at 10 (■), 15 (●), 20 (▲), 25 (▼), and 30 °C (♦): (a) G' vs G'' and (b) G' and G'' vs the shifted frequency ($a_T\omega$). The shifting in (b) was carried out by superposing the data at the high-frequency limit, with 15 °C as the reference temperature.

TABLE I. Generalized Maxwell fits to linear viscoelastic data.

	10 °C	15 °C	20 °C	25 °C	30 °C
$\lambda_i = 30$ s	$\eta_i = 61.8$ Pa s	⋯	⋯	⋯	⋯
10 s	76.5	17.5 Pa s	⋯	⋯	⋯
3 s	16.8	33.9	6.21 Pa s	⋯	⋯
1 s	20.3	7.0	12.5	2.74 Pa s	⋯
0.3 s	6.09	5.22	3.51	5.61	2.02 Pa s
0.1 s	7.75	5.62	3.51	1.9	2.06
0.01 s	6.95	4.1	2.77	2.07	1.49
0 s	$\eta_s = 16.4$	10	5.9	3.73	2.42
$\bar{\lambda}$	12.7 s	3.43 s	0.946 s	0.289 s	0.104 s

shown in Fig. 5(b). The viscoelastic response of the bicontinuous microemulsion is quite similar to that observed for undiluted block copolymer melts [Rosedale and Bates (1990); Almdal *et al.* (1990)] and block copolymer solutions [Jin and Lodge (1997)] just above the order–disorder transition temperature. The reduced frequency plots show terminal linear viscoelastic behavior with $G' \sim \omega^2$ and $G'' \sim \omega$ in the limit $\omega \to 0$.

Oscillatory shear measurements on the pure homopolymers over the same frequency and temperature range show no measurable elastic response. Hence, the elasticity revealed in these experiments must be due to the microemulsion structure present in the ternary blend. The data presented in Figs. 4 and 5 can be fit to a generalized Maxwell model using two relaxation modes per decade (Table I). A viscous ''solvent'' mode (relaxation time $= 0$) must be added to properly represent the data. The main contribution to this mode is from the purely viscous response of the constituent homopolymers. There may also be a small contribution from the high frequency viscoelastic response due to the microemulsion structure (G' continues to increase at the highest accessible frequency, indicating fast-relaxing viscoelastic modes in the sample). Assuming, however, that this term is dominated by the rheology of the homopolymer constituents, we would anticipate that it would be close to a weighted average of the homopolymer viscosities. This solvent viscosity is plotted along with the homopolymer viscosities and the zero-shear viscosity of the bicontinuous microemulsion as a function of temperature in Fig. 6. The solvent viscosity that reflects the high frequency dynamics, does, indeed, lie between the homopolymer viscosities. Since PEE is relatively close to its glass transition ($T_g \cong -30\,°\mathrm{C}$), it exhibits a much higher viscosity than PDMS ($T_g \cong -125\,°\mathrm{C}$), and a stronger temperature dependence. Assuming that both components in the bicontinuous structure experience the same deformation, the simplest estimate for the ''composite'' viscosity would be

$$\eta_{\mathrm{mix}} = \phi_1 \eta_1 + \phi_2 \eta_2 . \tag{1}$$

Due to the dramatic contrast in viscosity between the two homopolymers, the purely viscous response of the microemulsion can be associated with a viscosity that is roughly half that of the PEE homopolymer. Similar reasoning suggests that the temperature dependence of η_{mix} should be dominated by the PEE component. Instead, we find that the high frequency microemulsion viscosity is closer to 20%–25% of the PEE, although Fig. 6 clearly shows that the temperature dependence of the high frequency viscosity closely parallels that of the PEE. The lower-than-expected viscosity may reflect incomplete segregation with PDMS acting as a plasticizer, thereby reducing the viscosity of the PEE-

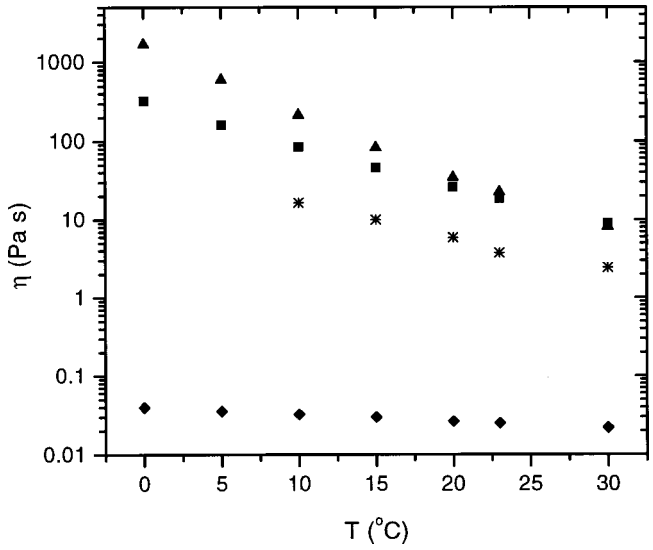

FIG. 6. Zero-shear viscosity plotted as a function of the temperature for the PDMS homopolymer (◆), the PEE homopolymer (■), and the bicontinuous microemulsion (▲), along with the ''solvent'' viscosity (*) used with the Maxwell model for fitting the data.

rich domain in the microemulsion. These arguments ignore the role of the PEE–PDMS diblock (10% of the total sample), although this should actually promote a *higher* viscosity because of its higher molecular weight and topological restriction to the interface.

Since the microemulsion does not follow time–temperature superposition, there is no unique way to characterize the temperature dependence of the sample. The two most meaningful measures would seem to be tracking the temperature dependence of the average relaxation time (using results from Table I) and the temperature dependence of the zero-shear viscosity (data from Fig. 6).

Given a discrete relaxation spectrum fit to the linear viscoelastic data, it is possible to compute an average relaxation time according to

$$\bar{\lambda} = \frac{\Sigma \lambda_i \eta_i}{\Sigma \eta_i}, \tag{2}$$

TABLE II. Shift factors for the rheology and structure of the PEE–PDMS microemulsion; $T_{\mathrm{ref}} = 15\,^{\circ}\mathrm{C}$.

	η_{PDMS}	η_{PEE}	$\eta_{s,b\mu E}$	$\eta_{0,b\mu E}$	$\bar{\lambda}_{b\mu E}$	Anisotropy index	Phase-separation index
0 °C	1.34	7.04	⋯	20.4	⋯		
5	1.20	3.52	⋯	7.32	⋯		
10	1.10	1.85	1.64	2.60	3.70	⋯	⋯
15	1.0	1.0	1.0	1.0	1.0	1.0	1.0
20	0.893	0.568	0.59	0.42	0.28	0.29	0.60
25	0.848	0.408	0.373	0.27	0.084	0.082	0.20
30	0.741	0.197	0.242	0.096	0.030	0.032	0.12
35	⋯	⋯	⋯	⋯	⋯	0.011	0.040
40	⋯	⋯	⋯	⋯	⋯	0.0059	0.020
45	⋯	⋯	⋯	⋯	⋯	0.0029	0.014

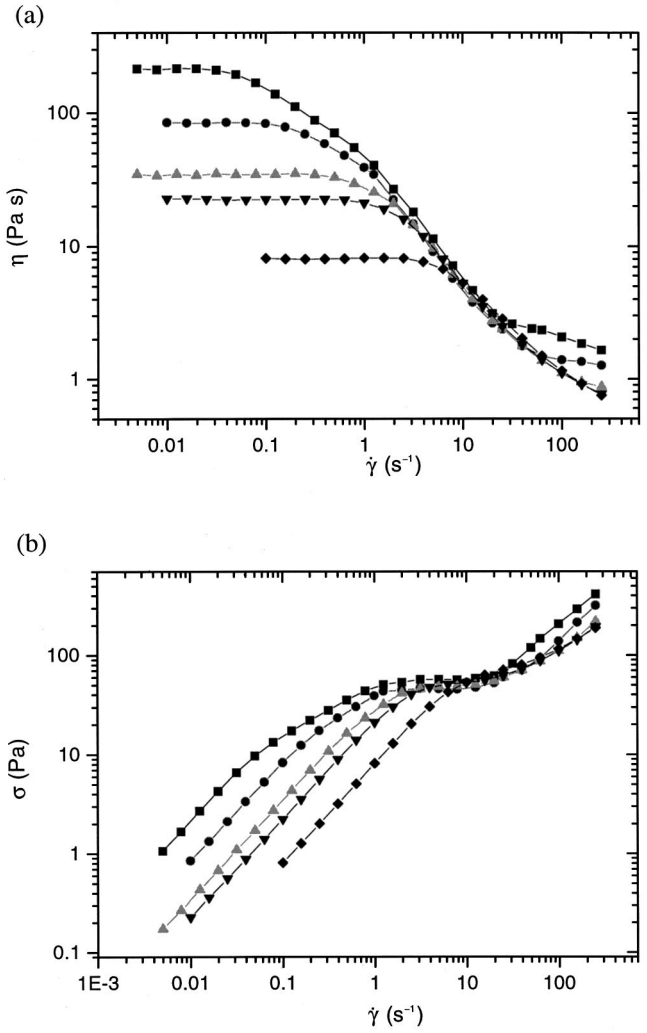

FIG. 7. Steady shear data on bicontinuous microemulsion at 10 (■), 15 (●), 20 (▲), 23 (▼), and 30 °C (♦): (a) viscosity vs the shear rate and (b) shear stress vs the shear rate.

where λ_i are the relaxation times and η_i the corresponding viscosities. Table II summarizes the temperature dependence of several quantities of interest, represented by shift factors relative to a reference temperature of 15 °C. Comparing the shift factors of the high frequency solvent viscosity to the PEE homopolymer viscosity confirms that they share a similar temperature dependence. Conversely, both the zero-shear viscosity of the microemulsion and its average relaxation time exhibit much stronger temperature dependences than either of the homopolymers. The ordinary temperature dependent *dynamics* of the constituent polymers are compounded by changes in the *thermodynamic* state of the system. As the temperature decreases, the degree of segregation between PEE and PDMS in the microemulsion increases, resulting in an increasingly well-defined (and elastic) interfacial structure, and greater barriers for diffusion except through the tortuous bicontinuous morphology. The strong temperature dependence of the average viscoelastic

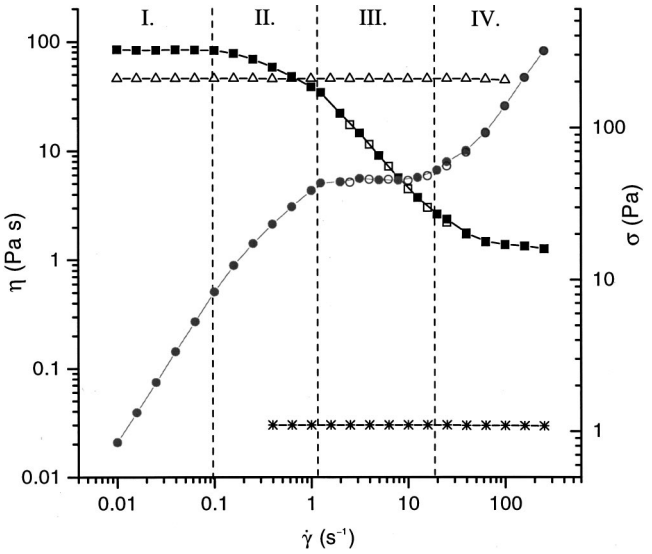

FIG. 8. Steady shear data of the bicontinuous microemulsion at 15 °C showing four regimes as a function of the shear rate. The plot shows the viscosity (■) and shear stress (●). Data collected in the reverse direction, i.e., with decreasing rates are shown by (□) and (○), respectively. The viscosities of homopolymers PEE (△) and PDMS (*) are also plotted for comparison.

relaxation time is particularly noteworthy: the relaxation time changes by two orders of magnitude over a span of just 20°.

Pätzold and Dawson (1996) presented a Landau–Ginzburg analysis of the dynamic linear viscoelasticity associated with small amplitude sinusoidal deformation of a bicontinuous microemulsion. The predicted behavior is, in gross terms, similar to the Rouse model: terminal relaxation at low frequencies, and $G' = G'' \sim \omega^{1/2}$ ($\delta = 45°$) at high

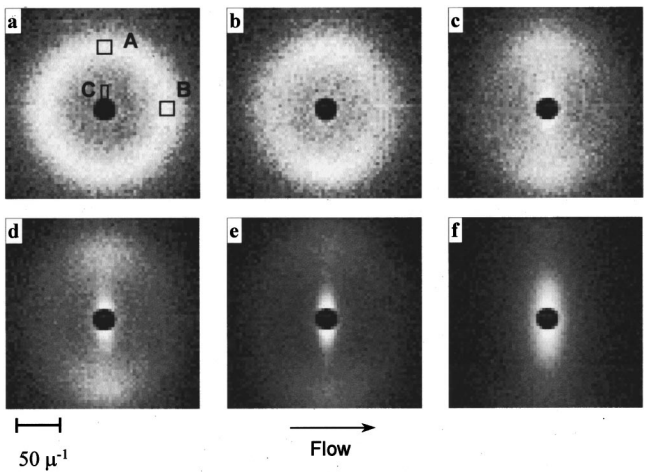

FIG. 9. Steady state SANS patterns at various shear rates ($T = 15$ °C): (a) 0 s^{-1}, (b) 0.316, (c) 3.16, (d) 10, (e) 31.6, and (f) 316 s^{-1}. The direction of flow is horizontal. The small boxes in (a) indicate the pixels used for calculating the anisotropy and phase-separation indices. The former is defined as $2B/(A+B)$ and the latter as $C(\dot{\gamma})/C(\dot{\gamma} = 0)$.

frequencies. In a real system, this would be accompanied by a viscous contribution from the pure components, which would enhance G' relative to G'' by a constant amount, and lead to an upturn in phase angle at high frequencies. Qualitatively, these predictions agree well with the behavior seen in Figs. 4 and 5; in particular, the high frequency G' data come close to exhibiting power law scaling with an exponent 1/2.

Steady shear rheological data also were collected at different temperatures and shear rates. Figure 7(a) shows the viscosity of the bicontinuous microemulsion as a function of shear rate $\dot{\gamma}$ at various temperatures. The corresponding stresses σ are shown in Fig. 7(b). These data are presented without any attempt at time–temperature shifting. A cursory comparison between Figs. 4 and 7 shows that the Cox–Merz rule [Cox and Merz (1958)] fails for the microemulsion. As will be shown below, this reflects radical steady shear-induced changes in the fluid structure at high rates. Four regimes can be identified as a function of the shear rate. Figure 8 depicts these four regimes at 15 °C. The viscosities of the homopolymers are also plotted for comparison.

The bicontinuous microemulsion shows Newtonian behavior at low shear rates, which is designated as regime I. Note that the zero-shear viscosity strongly decreases with the temperature [see Fig. 7(a)] due to the temperature dependence of the morphology of the bicontinuous microemulsion, as discussed earlier. Newtonian behavior persists up to the onset of shear thinning, which signals the beginning of regime II. Experiments conducted at other temperatures revealed that the critical shear rate for shear thinning increases with an increase in temperature (e.g., 0.03 s^{-1} at 10 °C; 0.1 s^{-1} at 15 °C), and also that the shear rate window for regime II narrows with an increase in temperature.

Regime III is characterized by a shear rate independent shear stress (i.e., the viscosity power law index $\cong -1$), and a marked enhancement in shear thinning. This dramatic change suggests a significant transformation in the morphology. Remarkably, the data collected at different temperatures almost overlap within regime III, indicating a stress level that is nearly independent of both the shear rate and the temperature. Increasing the shear rate further leads to an abrupt upturn in stress. We refer to this as regime IV. The rate dependence of η in this regime is much less than in regime III.

Significant normal stresses are also observed, particularly in regime IV. These are found to track the behavior of the shear stress in regime IV and in most of regime III. Even though the homopolymers do not show much elasticity, the presence of interfaces deformed by the shear flow leads to noticeable normal forces. However at lower shear rates the normal force falls below resolution of the instrument.

B. Small angle neutron scattering

SANS experiments were conducted with an *in situ* Couette flow shear cell operated at different temperatures and shear rates. Figure 9 shows representative scattering patterns obtained at 15 °C. In the quiescent state [Fig. 9(a)], a circular ring of scattering intensity is evident, characteristic of the bicontinuous microemulsion. The associated structure factor obeys the form [Teubner and Strey (1987)]

$$I(q) = \frac{1}{a_2 + c_1 q^2 + c_2 q^4}, \tag{3}$$

where $q = (4\pi/\lambda)\sin(\theta/2)$ is the scattering wave vector, θ is the scattering angle, and $I(q)$ is the azimuthally averaged one-dimensional scattered intensity. Two characteristic length scales can be obtained from the fitting parameters: a domain periodicity d and a correlation length scale ξ that reflects the short-range order among the domains; at 25 °C, $d = 74$ nm and $\xi = 32$ nm. In addition, an amphiphilicity factor f_a can be defined using

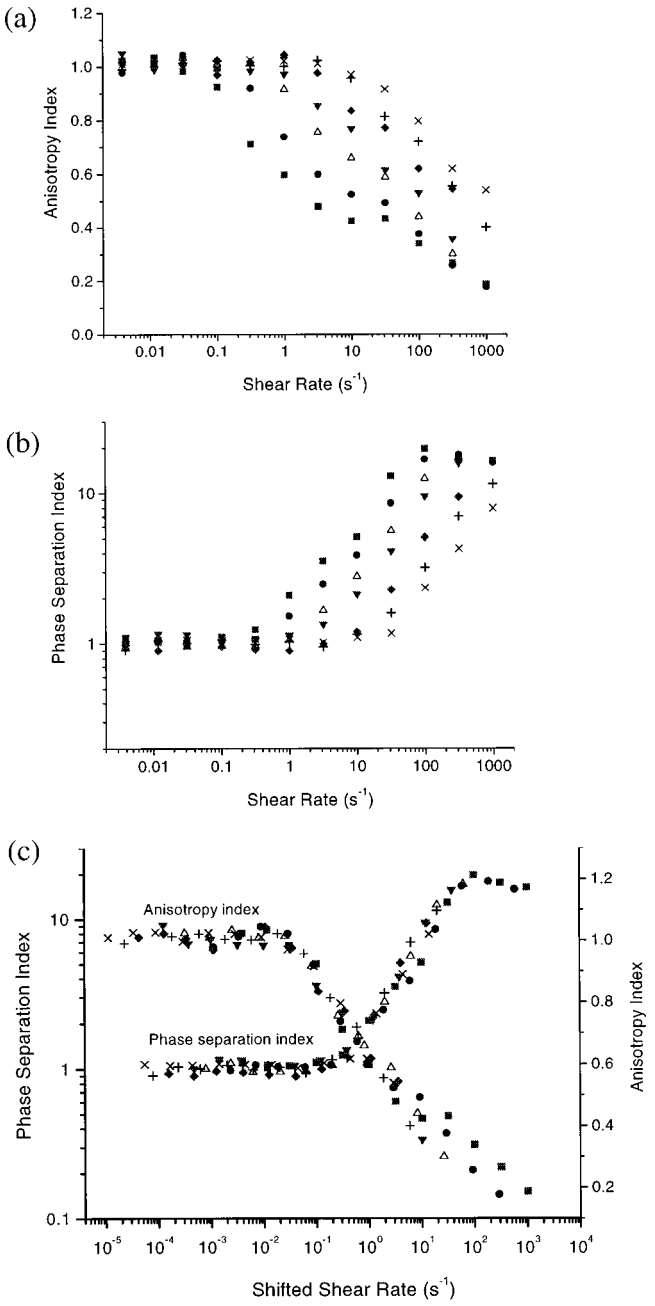

FIG. 10. Neutron scattering data analysis: (a) anisotropy index vs the shear rate, (b) phase-separation index vs the shear rate, and (c) indices vs the shifted shear rate at 15 (■), 20 (●), 25 (△), 30 (▼), 35 (♦), 40 (+), and 45 °C (×). The shifting in (c) was carried out by superimposing the data at the high shear rate limit and using 15 °C as the reference temperature.

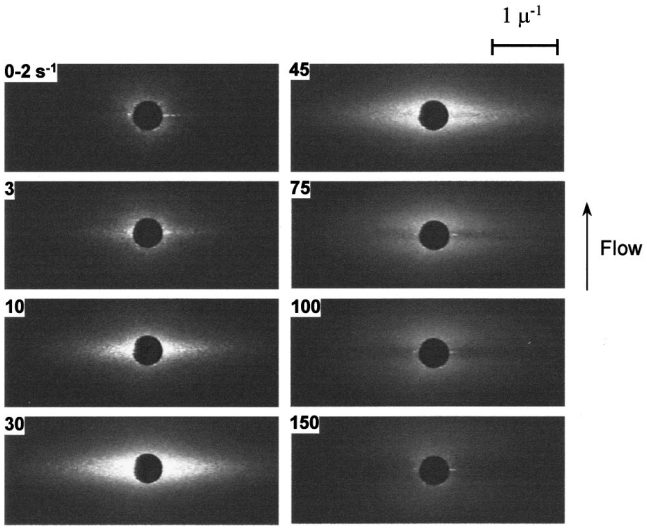

FIG. 11. Steady state light scattering patterns at various shear rates ($T = 15\,°\mathrm{C}$). The center dark region is due to the beamstop. The direction of flow is vertical.

the fitting parameters $[f_a = c_1/(4a_2c_2)^{1/2}]$ to classify the structure of the fluid. This number, which quantifies the degree of segregation between the domains [Schubert *et al.* (1994)] is negative and increases in magnitude as the microemulsion becomes more segregated at lower temperatures [see, for example, Morkved *et al.* (1999, 2001) for a fuller treatment of these thermodynamic properties].

At low shear rates, within regime I defined from rheology (Fig. 8), the SANS patterns are unperturbed by steady shear (i.e., they remain isotropic). Higher shear rates (regime II) produce anisotropy in the SANS patterns [Fig. 9(b)], with a loss of intensity along the flow direction. However, the q values associated with the intensity maxima in regime II are almost the same as in regime I, indicating that the concentration fluctuations with wave vectors parallel to the flow direction are suppressed by the shear flow, but that the structure is unperturbed along the vorticity direction. In regime III, intense low-q scattering develops around the beamstop, which increases with the shear rate [Figs. 9(c) and 9(d)]. Simultaneously the microemulsion scattering diminishes, first along the direction of flow, and then in all directions. Development of low-q scattering suggests the emergence of a morphology with a much larger length scale. This is indicative of *flow-induced phase separation* from a single bicontinuous microemulsion phase to a micron-scale multiphase state. This transition appears to be continuous, suggesting that the volume fraction of the microemulsion phase progressively decreases across regime III.

At very high shear rates, in regime IV, the microemulsion scattering completely disappears and only the strong low q scattering remains [Fig. 9(f)]. This low-q intensity grows to almost 10 times the intensity recorded for the unperturbed mixture. There is saturation in the scattering intensity at low q at these high rates. In fact, at 15 °C the low q intensity passes through a maximum at 100 s^{-1}, then decreases somewhat at still higher rates. An overall behavior pattern similar to that in Fig. 9 is also seen at other temperatures.

In order to quantify the SANS anisotropy in regime II, we define an ''anisotropy index.'' Figure 9(a) shows two small boxes labeled ''A'' and ''B'' within which average

intensities $\langle I \rangle$ are computed. We define the anisotropy index as $2\langle I \rangle_B / (\langle I \rangle_A + \langle I \rangle_B)$. The value of the index is unity for an isotropic pattern. Figure 10(a) depicts the anisotropy index as a function of the shear rate at various temperatures. There is a strong decrease in the index as the sample enters regime II.

A ''phase-separation index'' can be defined in a similar way. Figure 9(a) also shows a small box labeled ''C,'' which represents the detector pixels used in defining this index as $\langle I \rangle_C(\dot{\gamma}) / \langle I \rangle_C(\dot{\gamma} = 0)$. The index has a value of unity before the onset of phase separation. Figure 10(b) shows the phase-separation index plotted as a function of the shear rate. A marked increase in this index occurs in regimes III and IV.

Figure 10 is quite informative. First, a comparison of Figs. 10(a) and 10(b) shows that the temperature dependence of the development of anisotropy is stronger than the temperature dependence of the development of excess low-q scattering intensity. This may be quantified by exploiting the fact that the shapes of the curves in Figs. 10(a) and 10(b) are similar at all temperatures. Figure 10(c) presents a ''master plot'' obtained by shifting the data from Figs. 10(a) and 10(b). The shifting was carried out by superimposing the data at high shear rates using 15 °C as a reference temperature. Note that *separate* sets of shift factors were used to shift the anisotropy and phase separation data. The quality of the superposition is quite satisfying. Both sets of shift factors are listed in Table II. Several of the features referred to earlier are apparent. The transition from regime I to II is evident in the anisotropy index. The onset of phase separation, which we associate with the beginning of regime III, is signaled by the upturn in the phase-separation index. The saturation in low-q scattering at high shear rates is also evident. There is a slight mismatch between the critical shear rates for these transitions predicted by SANS and by rheology, the critical shear rates from the former being systematically less than those from the latter. This implies that neutron scattering is more sensitive to changes in structure than rheology. But the development of two different phenomena can clearly be seen from each of these two separate experiments.

C. Flow light scattering

Small angle light scattering provides access to much smaller q values, hence larger length scales than SANS. Light scattering experiments were carried out at various temperatures and shear rates using the procedures described in Sec. II. Figure 11 shows representative data at 15 °C. In the quiescent state, no significant light scattering was recorded, a consequence of the characteristic dimensions of the bicontinuous microemulsion. There was only a small amount of stray background scattering due to reflection from the optical elements. This lack of scattering persisted as the shear rate was increased through regimes I and II, consistent with the SANS analysis. Upon entering regime III($\dot{\gamma} \cong 1.5\ s^{-1}$), a streaked light scattering pattern emerged around the beamstop perpendicular to the direction of flow, which increased in intensity with an increase in the shear rate across regime III. The appearance of the bright streak coincides with the onset of the stress plateau in rheology (Fig. 8), and this critical shear rate increases with the temperature. Similar streak-like patterns have been reported in sheared polymer solutions [Kume *et al.* (1997)] and in blends [Hong *et al.* (1998); Kielhorn *et al.* (2000); Fernandez *et al.* (1995); Kim *et al.* (1997)] and attributed to the presence of a string-like morphology aligned along the direction of flow. Accurate quantitative analysis of the scattering intensity cannot be obtained with the present experimental setup. However the q range of the scattered intensity at these shear rates suggests a length scale on the order of microns, consistent with the hypothesis that flow-induced phase separation occurs in regime III, with phase-separated domains oriented along the direction of flow. Further increases in

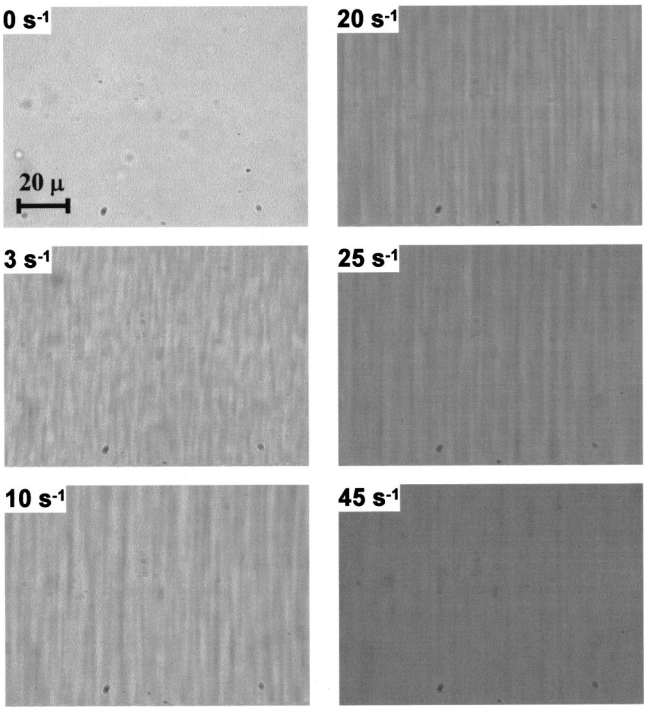

FIG. 12. Real-space steady state images of the bicontinuous microemulsion under shear at various shear rates ($T = 15\,°C$). The images have the same scale of intensity and become progressively darker with an increase in shear rate because of higher sample turbidity. The direction of flow is vertical.

the shear rate lead to loss in the overall intensity of the scattering images. This is due, at least in part, to increased turbidity of the sample. At shear rates well into regime IV($\dot{\gamma} > 20\ s^{-1}$), a dark streak is superimposed along the center line of the bright pattern. We return to this feature in Sec. IV. The dark streak separating the two lobes of scattered intensity becomes wider with an increase in shear rate, resulting in a butterfly-like pattern. As the shear rate increases, the wings of the butterfly move apart and ultimately disappear at the highest rates. In addition, the overall intensity of the patterns decreases with an increase in temperature. We attribute this last effect to a reduction in contrast, due to more mixing of the components.

Light scattering data were also collected during relaxation after shear. In regime III, cessation of steady shear led to a gradual retraction of the streak-like pattern into the beamstop that occurred over a period of 15–30 min, depending on the shear rate. In contrast, recovery from very high shear rates ($\sim 200\ s^{-1}$) in regime IV led to the immediate (1–2 s) development of isotropic scattering around the beamstop. The isotropic pattern gradually diminished in intensity and finally disappeared in about 20–30 min.

D. Optical microscopy

The bicontinuous microemulsion sample appears homogeneous and almost transparent to the naked eye, but has a faint blue tint due to scattering of light from the nanostructure. Rapid stirring makes the sample turbid, and the turbidity increases with the stirring rate. This, again, is indicative of flow-induced phase separation. More systematic measure-

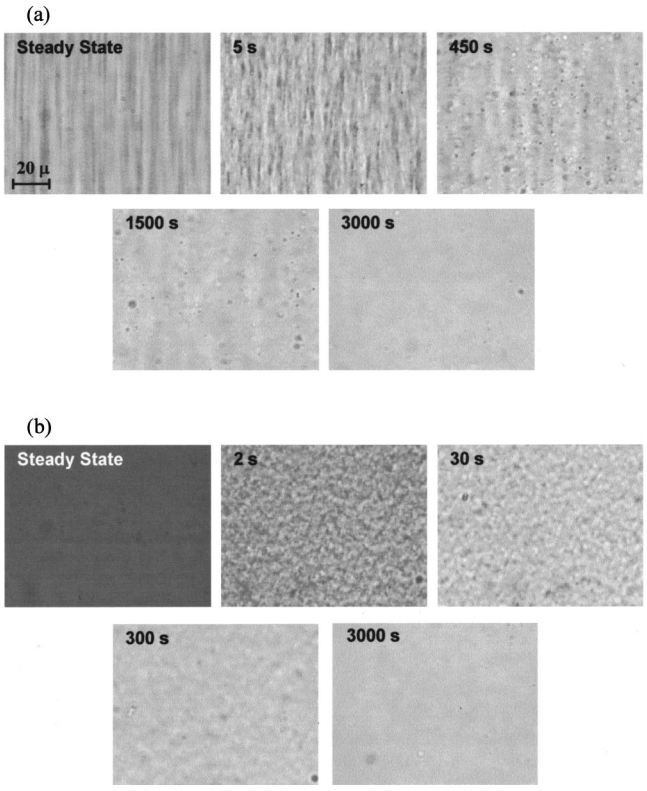

FIG. 13. Microscopy images of structural relaxation after cessation of shear flow at (a) 7.5 s^{-1} (regime III) and (b) 150 s^{-1} (regime IV). The numbers at top left-hand corner indicate the time after the cessation of shear. The intensity scale is same for all the images. The direction of flow is vertical.

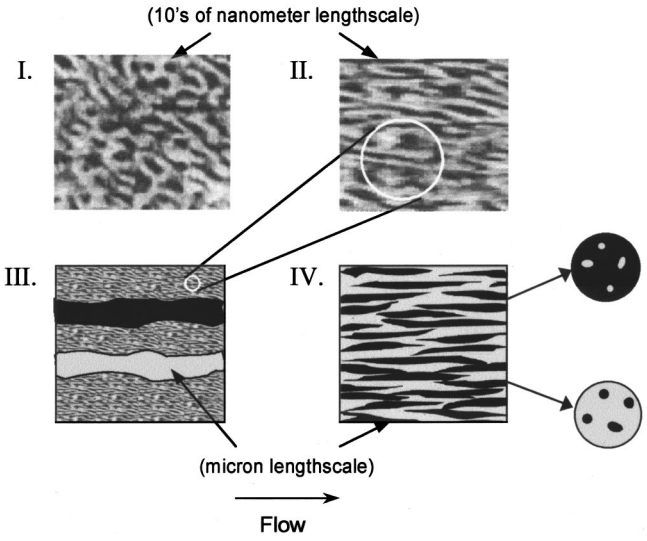

FIG. 14. Schematic representation of the morphology in the four regimes: I Newtonian regime, II development of anisotropy, III three-phase coexistence after the onset of phase separation, and IV binary blend-like behavior. The block copolymer is dispersed as micelles in the homopolymer-rich domains in regime IV.

ments were conducted by operating the shear stage under an optical microscope. Figure 12 illustrates the steady state morphologies obtained at 15 °C at various shear rates.

In the quiescent state, the sample is homogeneous (except for a few dust particles). Steady shear flow does not produce any significant change for shear rates corresponding to regimes I and II. However in regime III (shear rates 3, 10, and 20 s^{-1}), the turbidity of the sample increases, accompanied by the development of a string-like morphology aligned along the direction of flow. There is a drastic transformation from the nanometer-size microemulsion to this micron-size string-like phase. The turbidity further increases with the shear rate, as evidenced by a progressive darkening of the images. There also is an increase in the length scale along the direction of flow across this regime, as seen from the images in Fig. 12. Further increases in the shear rate in regime IV result in strong turbidity, and the images become very dark. Fine string-like structures still could be seen even at shear rates close to 100 s^{-1} when the illumination was increased. The sample thickness was reduced in order to obtain better images, since the velocities would be lower for a given shear rate there by overcoming limitations of the video recording system. However below a certain gap width spurious wall effects became evident.

Recovery of the microemulsion also was recorded after the cessation of shear flow. As noticed for the light scattering, the modes of recovery were very different at intermediate and high shear rates. Figure 13 illustrates the recovery after steady shearing at 7.5 and 150 s^{-1}. In the former case (regime III), the anisotropy in the morphology persists for a long time, and there is also formation of droplet-like structures due to retraction and breakup of the string-like domains. These structures gradually dissolve over a period of about 20–30 min. On the other hand, after cessation of shearing at 150 s^{-1} (regime IV), there was an immediate increase in the overall brightness of the image, followed by the formation of a nearly isotropic grain-like structure, slightly elongated along the direction of flow. These structures resemble the spinodal-type phase-separated domains that are seen in binary polymer blends after cessation of shear at high rates [Kielhorn *et al.* (2000)]. These structures appear within seconds, whereas the droplets in regime III take a few minutes to develop. The grain-like structures coarsen, and simultaneously the interfaces become hazier. The sample reaches the original homogeneous state in about 45 min.

Turbidity measurements were performed using the light scattering setup by measuring the transmitted intensity (i.e., without the beamstop) using a photodiode. The photodiode gives a voltage signal that is proportional to the intensity. A nearly constant intensity was recorded in regimes I and II, and a sharp drop was observed in regime III, clearly due to phase separation. The intensity transmitted progressively decreased with an increase in shear rate across regime III, ultimately reaching a steady value. This increase in turbidity confirms our speculation regarding the loss of brightness found in the microscopy images in Fig. 12. The absolute magnitude of the scattered intensity in regime III, of course, strongly decreases with an increase in sample thickness.

IV. DISCUSSION

This polymeric bicontinuous microemulsion clearly exhibits rich rheological phenomena; four regimes are observed as a function of the shear rate. We associate different morphologies with these regimes, as depicted in Fig. 14; various experimental techniques have been used, each one providing a different perspective on the flow-induced transformations of the structure. Here in Sec. IV we provide justification for the proposed structure in each of these regimes; analogies are also drawn with both block copolymer mesophases and immiscible polymer blends.

A. Regime I

Steady shear rheology was used to establish a Newtonian behavior in regime I. The characteristic time scales of the experiment were much longer than the relaxation time of the microemulsion, resulting in a liquid-like response. This was confirmed by the *in situ* SANS experiment, where the isotropic diffraction ring resulting from the bicontinuous microemulsion was unaffected by Couette flow. From this we deduced that the morphology was unperturbed (Fig. 14) in this regime.

The linear dynamic mechanical data from the bicontinuous microemulsion are remarkably similar to the rheological response of symmetric lamellar forming block copolymers just above the order–disorder transition (T_{ODT}), for example, reported by Rosedale and Bates (1990) for poly(ethylene propylene) (PEP)–poly(ethyl ethylene) block copolymers. With block copolymers, terminal viscoelastic behavior ($G' \sim \omega^2$ and $G'' \sim \omega$) was obtained at temperatures well into the disordered phase, whereas below T_{ODT}, the scaling followed $G' \sim G'' \sim \omega^{0.5}$. Near T_{ODT}, a lack of superimposability at low frequencies characterized the viscoelastic response, and this has been attributed to fluctuation effects. Because the amplitude of these composition fluctuations is temperature dependent, and because it also influences the level of sustainable stress (i.e., G'), fluctuating block copolymer melts become thermorheologically complex. Our data on the bicontinuous microemulsions (Fig. 5) closely resemble the fluctuation dominated disordered state block copolymer response.

This kind of a response can be understood by treating the bicontinuous microemulsion channel as an extension of a ''band'' of fluctuations around the T_{ODT} of the lamellar phase. Consider the phase diagram in Fig. 1(b). At the pure block copolymer limit, the system self-assembles into a lamellar phase. The addition of homopolymers swells this phase. The lamellar spacing progressively increases with the added homopolymers, ultimately resulting in phase separation. However phase separation is pre-empted by the fluctuation-induced formation of a bicontinuous microemulsion. This happens when the swelling reaches a point where the interfaces are sufficiently separated that they lose orientational correlation [Matsen (1999)]. Around the order–disorder transition boundary, there exists a band of strong fluctuations (this band leads to suppression of lamellar phase formation as the temperature is decreased through the ODT). We envision the bicontinuous microemulsion channel as an extension of this band of fluctuations; the resemblance of our rheological data with those on lamellar block copolymers supports this notion.

Failure of time–temperature superposition in the microemulsion means that there is some subtlety to the temperature dependence of the structural dynamics and rheology of this sample. Three relaxation phenomena with distinctly different temperature dependences are discernible. The first two, which concern the average relaxation time computed from the linear viscoelastic spectrum and the zero-shear viscosity, are related to the macroscopic response of the microemulsion. The third one, the high frequency viscous response, is related to the relaxation at the molecular level. Connections can be made between the rheology and SANS data to better understand these phenomena.

The average relaxation time of the microemulsion structure [see Eq. (2)] exhibits the strongest temperature dependence. Examination of Table II shows that the temperature dependence of the development of anisotropy in the neutron scattering tracks that of the average relaxation time (shift factors for $\bar{\lambda}$ lead to an apparent activation energy of 170 kJ/mol, while shift factors for the anisotropy index lead to an apparent activation energy of 150 kJ/mol). In order to obtain coupling between the structure and flow, and thus scattering anisotropy, the shear rate must exceed the inverse of the microemulsion relaxation time. These two processes could be characterized by a type of Weisenberg number

(bearing in mind that we are dealing with the *microemulsion* relaxation time; the *molecular* relaxation times of the polymer constituents are much smaller).

The zero-shear viscosity is also strongly temperature dependent, although somewhat less so than the average relaxation time. It appears that the temperature dependence of the phase-separation index as documented by neutron scattering (activation energy of 115 kJ/mol) is equivalent to that of the microemulsion zero-shear viscosity (activation energy of 120 kJ/mol). This similarity suggests that the phase-separation process is activated by a critical *stress level* rather than by achieving a critical Weisenberg number (in ordinary polymers these two criteria would be identical; they are different here due to the complexity of this sample). In fact, this idea is more forcefully supported by the connection between the observed phase separation and the stress plateau seen in steady shear, which will be discussed further. Finally, the viscous response at high frequency exhibits a temperature dependence that is intermediate between those of the constituent homopolymers, but closer to PEE, due to the fact that its high viscosity dominates the purely viscous response of the microemulsion (Fig. 6).

B. Regime II

Upon entering regime II, anisotropy develops in the morphology (Fig. 14). The domains that are initially oriented perpendicular to the direction of flow tend to be rotated away due to the shear flow. As a result, there is suppression of concentration fluctuations along the direction of flow and the SANS patterns become anisotropic. Complementary SANS experiments (not shown) with the beam directed tangential to the Couette cell (see Fig. 2) confirm these results. The anisotropy leads to a decrease in the degree of percolation of the bicontinuous structures along the direction of the velocity gradient. This gives rise to shear thinning, particularly because there is great contrast between the viscosity of the two homopolymers. It is worth noting that there is only a superficial similarity between the elongated structures in the microemulsion and worm-like surfactant micelles (''living polymers''). Although both exhibit shear thinning due to orientation, the microemulsion shows no signature of entanglement or the single relaxation time, i.e., Maxwellian response [Cates (1987)] of ''living'' polymers.

C. Regime III

As described in Sec. I, the bicontinuous microemulsion is located in a narrow composition range between lamellar and phase-separated states. One might expect, therefore, that shear flow could lead the sample to become either lamellar or phase separated in a fashion analogous to that of flow-induced shifts in the phase boundaries observed for binary polymer blends. Studies on related soft materials (sponge phases and block copolymers, for example) have indicated a transition from an isotropic to a lamellar state, as discussed in Sec. I. In contrast, shear flow of the bicontinuous microemulsion leads to phase separation after reaching a critical shear stress. We hypothesize that the microemulsion ejects two homopolymer-rich phases when the stress exceeds this critical value. Some block copolymer is also expelled and is distributed between the homopolymer-rich phases, with the remainder still lying at the interfaces between domains. We thus expect three-phase coexistence in regime III as illustrated in Fig. 14, the bicontinuous microemulsion and two homopolymer-rich phases. With an increase in shear rate across regime III, the extent of phase separation progressively increases, while maintaining a constant stress. SANS and SALS results show the concurrent development of strong low-q scattering, which indicates a dramatic increase in the structural length scale. They also indi-

cate remnants of scattering intensity in the q range of the bicontinuous microemulsion, thus supporting the argument for three-phase coexistence.

Flow-induced phase separation also can be rationalized in terms of movement across phase boundaries. This is equivalent to moving downward in the isothermal phase diagram [Fig. 1(a)] from the bicontinuous microemulsion region, first into the three-phase triangle, and then into the two-phase region when the shear rates reach regime IV. In terms of the phase diagram along the isopleth [Fig. 1(b)], this corresponds to horizontal movement from the microemulsion channel into the phase-separated regime.

The progressive increase in the degree of phase separation across regime III is documented by optical microscopy. These experiments reveal string-like structures as a result of phase separation, with the number of strings or the amount of homopolymer-rich phases increasing with the shear rate. This is accompanied by a strong growth in turbidity. SALS experiments also support this argument, with the formation of a streak-like pattern at the onset of phase separation and a progressive increase in intensity with the shear rate across regime III.

The shear-induced anisotropy persists for a long time after flow is brought to an abrupt halt. This includes the formation of droplet-like structures by the retraction and breakup of the strings and a general nonrandom distribution of the domains. Based on these observations, we may conclude that the string-like phase in regime III arises from true phase separation and is not due to flow instabilities such as those reported by Fernandez *et al.* (1995).

The stress level corresponding to the plateau, in addition to being independent of the shear rate, is also nearly independent of the temperature; the reason for this is not clear at present. The onset of the stress plateau also roughly corresponds to the shear rate when the viscosity of the bicontinuous microemulsion becomes equal to that of the homopolymer PEE. Stress plateaus have been reported in several other complex fluids. In the case of worm-like micelles, Spenley *et al.* (1993) explained the plateau on the basis of a nonmonotonic dependence of stress on the shear rate in a single fluid phase, resulting in shear banding instability; Olmsted and Lu (1997, 1999) and Berret *et al.* (1994, 1998) interpreted the stress plateau in similar systems in terms of a transition between an isotropic and a nematic phase, with the plateau representing the two-phase region. In our system, the plateau corresponds to breakdown of the microemulsion and represents the transition between the bicontinuous and completely phase-separated states. Unlike other systems, there is no layer or band formation along the direction of the shear gradient; instead there is the development of string-like morphology. The stress plateau is robust and no hysteresis effects are observed. Long time transients are observed in the rheological behavior upon the inception of flow in the stress plateau. They show a remarkable resemblance to worm-like micelles and will be presented in a future publication. In the case of worm-like micelles, the nematic phase has a much lower viscosity than the isotropic phase. Similar rheological properties are observed for the bicontinuous microemulsion when the system undergoes phase separation and ejects low viscosity material.

D. Regime IV

Well into regime IV, the SANS patterns show complete loss of intensity at the microemulsion q range. We therefore propose that there is complete decomposition of the bicontinuous microemulsion into two homopolymer-rich phases in this regime. The block copolymer assumes a relatively minor role, and either resides in the interfaces or becomes solubilized (perhaps as micelles) in the homopolymer-rich phases (Fig. 14). Hence the sample behaves just like a typical binary polymer blend; the stress increases with the shear rate, albeit accompanied by some shear thinning [Veenstra *et al.* (1999); Miles and

Zurek (1988)]. In SALS experiments a dark streak is seen in the middle of the bright pattern when the shear rates are well inside regime IV. At very high rates, the scattering pattern resembles a butterfly. There also is an overall decrease in the intensity of the patterns at these high rates, probably due to high turbidity and multiple scattering.

Butterfly-like SALS patterns similar to those in our experiments have been reported for polymer blends only in the case of transient evolution of bright streak patterns [Hong *et al.* (1998, 2000); Chen *et al.* (1995)]. In our system, this pattern occurs at *steady state* [the well-known steady state butterfly patterns in semidilute polymer solutions reported by Moses *et al.* (1994) and by Kume *et al.* (1997) are qualitatively different]. Hong *et al.* (1998, 2000) have attributed some of their butterfly patterns to a chevron-like morphology. This structure arises because of the development of secondary flow with a velocity component in the vorticity direction. The superposition of primary and secondary flows results in helical flow. The projection of helical flow on a plane perpendicular to the beam would show chevron-like structures that produce a butterfly-like scattering pattern.

An alternative explanation invokes a change in length scale as a function of the shear rate [Chen *et al.* (1995)]. One can imagine the butterfly pattern as being a ''squashed'' spinodal ring, with the distance between the intensity maxima in the two directions being inversely proportional to the respective length scales. In the case of a bright streak pattern, the length scale along the direction of flow is so large that the wings of the butterfly almost touch each other and the dark streak in the middle is not visible. When there is breakage of strings at high rates, and hence a reduction in the length scale along the direction of flow, the dark streak can easily be seen. It is unclear at present whether these explanations based on transient patterns are applicable to the steady state.

Microscopic observations are difficult in regime IV due to the high velocity of the strings and the strong turbidity. Increasing the illumination helped us to discern fine ($< 1\ \mu$m) strings even at rates close to 100 s^{-1} at 15 °C. Stopping the shear leads to the immediate formation of fine grain-like structures [Fig. 13(b)]. These structures coarsen initially; then the interfaces become hazy, ultimately leading to a homogeneous bicontinuous microemulsion phase. One can call this kind of phenomenon ''reverse spinodal decomposition.'' The mechanism for the appearance of the spinodal-like morphology is not fully understood. Our experiments produce results that resemble the behavior of immiscible polymer blends reported by Kielhorn *et al.* (2000). A plausible explanation for this strange relaxation behavior is that the strings, which are finer at higher rates, break up into many tiny droplets due to Rayleigh instability, and rapidly coalesce with adjacent droplets. The connection to neighboring droplets results in a spinodal-like morphology. Another possible explanation is that the radius of the droplets that appear upon cessation of the shear after near homogenization by shearing, is smaller than the critical radius for domain growth and as a result they dissolve immediately. A spinodal decomposition-like phenomenon follows this, yielding a fine-grain structure [Kielhorn *et al.* (2000)]. This kind of relaxation behavior which is analogous to that of immiscible blends, supports our argument of complete phase separation in regime IV. Upon the cessation of shear, the short-time response is that of a binary blend, and the system attempts to form macroscopically phase-separated domains via spinodal decomposition. However the system soon recognizes the presence of the block copolymer, which starts diffusing towards the interfaces to form the bicontinuous microemulsion. Two competing phenomena are thus observed: at short times the phase separation through spinodal decomposition is dominant, whereas over longer periods homogenization into bicontinuous microemulsion triumphs. In terms of free energy, the local minimum is the macroscopically phase-separated state whereas the global minimum is the bicontinuous microemulsion phase.

The transition between regimes III and IV is intriguing. SANS shows remnants of the bicontinuous microemulsion even after there is an upturn in stress. It is not clear whether the transition between the two regimes is the point at which there is complete phase separation, or the rate at which the bicontinuous microemulsion no longer remains continuous phase (and hence no longer controls stress in the sample).

E. Comparison with surfactants

Studies of sponge phases [Yamamoto and Tanaka (1996); Mahjoub *et al.* (1998)] have indicated a shear-induced transition to lamellar phase. It is unclear why the sponge phase becomes lamellar whereas the bicontinuous microemulsion prefers to phase separate. Oil/water/surfactant bicontinuous microemulsions show shear thinning only at very high shear rates [Anklam *et al.* (1995); Thevenin *et al.* (1999)]. This is interpreted in terms of the shrinking of conduits along the direction of the shear gradient and their subsequent pinching off. The shear rates for the onset of shear thinning were of the order of 10^3–10^4 s^{-1} in the o/w/s case whereas in our system it was of the order of 0.1 s^{-1}. This implies that the characteristic relaxation times in the two systems differ by several orders of magnitude. Studies of oil/water/surfactant bicontinuous microemulsions have been hindered by the necessity to use very high shear rates. This problem is overcome by the use of polymers. In addition, the polymeric system presents an opportunity by which to systematically change the ''strength'' or degree of segregation of the domains of the microemulsion by varying the temperature. In the o/w/s systems, the temperature–composition phase plane, often called a ''fish plot'' [Gompper and Schick (1994)] has a narrow range of temperatures over which the bicontinuous microemulsion exists. This precludes any attempt to study the effects of temperature on the rheological properties. Hence ternary polymer blends present many advantages over conventional o/w/s systems.

V. CONCLUSION

The model polymeric bicontinuous microemulsion under study exhibits four regimes as a function of the shear rate. Regime I resembles conventional Newtonian fluids. In regime II, there is an onset of anisotropy and shear thinning. Unlike the surfactant sponge phase, there is no transition to lamellar phase, instead the system undergoes phase separation upon entering regime III. The stress is independent of the shear rate, and this stress plateau resembles the behavior of worm-like micelles. There is complete phase separation in regime IV and the rheological properties become similar to those of binary polymer blends. We have thus established that polymeric bicontinuous microemulsions possess rich rheological behavior within accessible shear rates, and hence can serve as excellent model systems for studying the rheology and dynamics of this class of complex fluids.

ACKNOWLEDGMENTS

The authors would like to thank David Giles for assistance with rheological measurements, Tanya Slawecki for help with SANS, and David Morse, Jean-François Berret, and Franklin Caputo for useful discussions. This work was supported by the MRSEC program of the National Science Foundation under Award No. DMR-9809364, at the University of Minnesota.

References

Almdal, K., J. H. Rosedale, and F. S. Bates, ''The order–disorder transition in binary mixtures of nearly symmetric diblock copolymers,'' Macromolecules **23**, 4336–4338 (1990).

Anklam, M. R., R. K. Prud'homme, and G. G. Warr, ''Shear thinning in ternary bicontinuous and water-in-oil microemulsions,'' AIChE J. **41**, 677–682 (1995).

Bates, F. S., W. W. Maurer, P. M. Lipic, M. A. Hillmyer, K. S. Almdal, K. Mortensen, G. H. Fredrickson, and T. P. Lodge, ''Polymeric bicontinuous microemulsions,'' Phys. Rev. Lett. **79**, 849–852 (1997).

Berret, J.-F., D. C. Roux, and P. Lindner, ''Structure and rheology of concentrated wormlike micelles at the shear-induced isotropic-to-nematic transition,'' Eur. Phys. J. B **5**, 67–77 (1998).

Berret, J.-F., D. C. Roux, and G. Porte, ''Isotropic to nematic transition in wormlike micelles under shear,'' J. Phys. II **4**, 1261–1279 (1994).

Cates, M. E., ''Reptation of living polymers—Dynamics of entangled polymers in the presence of reversible chain-scission reactions,'' Macromolecules **20**, 2289–2296 (1987).

Cates, M. E. and S. T. Milner, ''Role of shear in isotropic-to-lamellar transition,'' Phys. Rev. Lett. **62**, 1856–1859 (1989).

Chen, C.-M. and G. G. Warr, ''Rheology of ternary microemulsions,'' J. Phys. Chem. **96**, 9492–9497 (1992).

Chen, Z. J., M. T. Shaw, and R. A. Weiss, ''Explanation of 'dark-streak' light scattering patterns and shear-induced structure development of phase-separated polymer blends,'' Macromolecules **28**, 648–650 (1995).

Chopra, D., D. Vlassopoulos, and S. G. Hatzikiriakos, ''Shear-induced mixing and demixing in poly(styrene-co-maleic anhydride)/poly(methyl methacrylate) blends,'' J. Rheol. **42**, 1227–1247 (1998).

Cox, W. P. and E. H. Merz, ''Correlation of dynamic and steady flow viscosities,'' J. Polym. Sci. **28**, 619–621 (1958).

Fernandez, M. L., J. S. Higgins, and M. Richardson, ''Flow instabilities in polymer blends under shear,'' Polymer **36**, 931–939 (1995).

Fredrickson, G. H., ''Steady shear alignment of block copolymers near the isotropic-lamellar transition,'' J. Rheol. **38**, 1045–1067 (1994).

Fredrickson, G. H. and F. S. Bates, ''Design of bicontinuous polymeric microemulsions,'' J. Polym. Sci., Part B: Polym. Phys. **35**, 2775–2786 (1997).

Gerard, H., J. S. Higgins, and N. Clarke, ''Shear-induced demixing in poly(styrene)/poly(vinyl methyl ether) blends. 1. Early stages of shear-induced demixing,'' Macromolecules **32**, 5411–5422 (1999).

Gompper, G. and M. Schick, *Phase Transitions and Critical Phenomena* (Academic, London, 1994), Vol. 16.

Gupta, V. K., R. Krishnamoorti, J. A. Kornfield, and S. D. Smith, ''Evolution of microstructure during shear alignment in a polystyrene-polyisoprene lamellar diblock copolymer,'' Macromolecules **28**, 4464–4474 (1995).

Han, C. D., D. M. Baek, J. K. Kim, T. Ogawa, N. Sakamoto, and T. Hashimoto, ''Effect of volume fraction on the order–disorder transition in low molecular weight polysterene-*block*-polyisoprene copolymers. 1. Order–disorder transition temperature determined by rheological measurements,'' Macromolecules **28**, 5043–5062 (1995).

Hashimoto, T., T. Takebe, and S. Suchiro, ''Ordered structure and critical phenomena of a semidilute solution of polymer mixtures under shear flow,'' J. Chem. Phys. **88**, 5874–5881 (1988).

Hillmyer, M. A., W. W. Maurer, T. P. Lodge, F. S. Bates, and K. Almdal, ''Model bicontinuous microemulsions in ternary homopolymer/block copolymer blends,'' J. Phys. Chem. B **103**, 4814–4824 (1999).

Hindawi, I. A., J. S. Higgins, and R. A. Weiss, ''Flow-induced mixing and demixing in polymer blends,'' Polymer **33**, 2522–2529 (1992).

Hong, Z., M. T. Shaw, and R. A. Weiss, ''Effect of shear flow on the morphology and phase behavior of a near-critical SAN/PMMA blend,'' Macromolecules **31**, 6211–6216 (1998).

Hong, Z., M. T. Shaw, and R. A. Weiss, ''Structure evolution and phase behavior of polymer blends under the influence of shear,'' Polymer **41**, 5895–5902 (2000).

Jin, X. and T. P. Lodge, ''Fluctuation regime in the viscoelastic properties of block copolymer solutions,'' Rheol. Acta **36**, 229–238 (1997).

Kielhorn, L. and M. Muthukumar, ''Fluctuation theory of diblock copolymer/homopolymer blends and its effects on the Lifshitz point,'' J. Chem. Phys. **107**, 5588–5608 (1997).

Kielhorn, L., R. H. Colby, and C. C. Han, ''Relaxation behavior of polymer blends after the cessation of shear,'' Macromolecules **33**, 2486–2496 (2000).

Kim, S., E. K. Hobbie, J.-W. Yu, and C. C. Han, ''Droplet breakup and shear-induced mixing in critical polymer blends,'' Macromolecules **30**, 8245–8253 (1997).

Koppi, K. A., M. Tirrell, F. S. Bates, K. Almdal, and R. H. Colby, ''Lamellae orientation in dynamically sheared diblock copolymer melts,'' J. Phys. II **2**, 1941–1959 (1992).

Koppi, K. A., M. Tirrell, and F. S. Bates, ''Shear-induced isotropic-to-lamellar transition,'' Phys. Rev. Lett. **70**, 1449–1452 (1993).

Krishnan, K., K. Almdal, T. P. Lodge, F. S. Bates, and W. R. Burghardt, ''Shear-induced nano–macrostructural transition in a polymeric bicontinuous microemulsion,'' Phys. Rev. Lett. **87**, 098301/1–098301/4 (2001).

Kume, T., T. Hattori, and T. Hashimoto, ''Time evolution of shear-induced structures in semidilute polystyrene blends,'' Macromolecules **30**, 427–434 (1997).

Mahjoub, H. F., C. Bourgaux, P. Sergot, and M. Kleman, ''Evidence of a sponge-to-lamellar phase transition under shear by x-ray scattering experiments in a couette cell,'' Phys. Rev. Lett. **81**, 2076–2079 (1998).

Martys, N. S. and J. F. Douglas, ''Critical properties and phase separation in lattice Boltzmann fluid mixtures,'' Phys. Rev. E **63**, 031205/1–031205/18 (2001).

Matsen, M. W., ''Elastic properties of a diblock copolymer monolayer and their relevance to bicontinuous microemulsion,'' J. Chem. Phys. **110**, 4658–4667 (1999).

Menasveta, M. J. and D. A. Hoagland, ''Light scattering from dilute poly(styrene) solutions in uniaxial elongational flow,'' Macromolecules **24**, 3427–3433 (1991).

Migler, K., C.-H. Liu, and D. J. Pine, ''Structure evolution of a polymer solution at high shear rates,'' Macromolecules **29**, 1422–1432 (1996).

Miles, I. S. and A. Zurek, ''Preparation, structure, and properties of two-phase co-continuous polymer blends,'' Polym. Eng. Sci. **28**, 796–805 (1988).

Morkved, T. L., B. R. Chapman, F. S. Bates, and T. P. Lodge, ''Dynamics of ternary polymer blends: Disordered, ordered and bicontinuous microemulsion phases,'' Faraday Discuss. **112**, 335–350 (1999).

Morkved, T. L., P. Stepanek, K. Krishnan, F. S. Bates, and T. P. Lodge, ''Static and dynamic scattering from ternary polymer blends: Lifshitz lines, disorder lines and bicontinuous microemulsion,'' J. Chem. Phys. **114**, 7247–7259 (2001).

Moses, E., T. Kume, and T. Hashimoto, ''Shear microscopy of the 'butterfly pattern' in polymer mixtures,'' Phys. Rev. Lett. **72**, 2037–2040 (1994).

Nakatani, A. I., L. Sung, E. K. Hobbie, and C. C. Han, ''Shear-induced order in a homopolymer blend with a block copolymer surfactant,'' Phys. Rev. Lett. **79**, 4693–4696 (1997).

Nakatani, A. I., H. Kim, Y. Takahashi, Y. Matsushita, A. Takano, B. Bauer, and C. C. Han, ''Shear stabilization of critical fluctuations in bulk polymer blends studied by small-angle neutron scattering,'' J. Chem. Phys. **93**, 795–810 (1990).

Olmsted, P. D., ''Two-state shear diagrams for complex fluids in shear flow,'' Europhys. Lett. **48**, 339–345 (1999).

Olmsted, P. D. and C.-Y. D. Lu, ''Co-existence and phase separation in sheared complex fluids,'' Phys. Rev. E **56**, R55–R58 (1997).

Pätzold, G. and K. Dawson, ''Connection of microstructure to rheology in a microemulsion model,'' Phys. Rev. E **54**, 1669–1682 (1996).

Rosedale, J. H. and F. S. Bates, ''Rheology of ordered and disordered symmetric poly(ethylenepropylene)-poly(ethylethylene) diblock copolymers,'' Macromolecules **23**, 2329–2338 (1990).

Schubert, K. V., R. Strey, S. R. Kline, and E. W. Kaler, ''Small angle neutron scattering near Lifshitz lines: Transition from weakly structured mixtures to microemulsions,'' J. Chem. Phys. **101**, 5343–5355 (1994).

Scriven, L. E., ''Equilibrium bicontinuous structure,'' Nature (London) **263**, 123–125 (1976).

Spenley, N. A., M. E. Cates, and T. C. B. McLeish, ''Nonlinear rheology of wormlike micelles,'' Phys. Rev. Lett. **71**, 939–942 (1993).

Tepe, T., D. A. Hajduk, M. A. Hillmyer, P. A. Weimann, M. Tirrell, and F. S. Bates, ''Influence of shear on a lamellar triblock copolymer near the order–disorder transition,'' J. Rheol. **41**, 1147–1171 (1997).

Teubner, M. and R. Strey, ''Origin of scattering peak in microemulsions,'' J. Chem. Phys. **87**, 3195–3200 (1987).

Thevenin, M. A. B., J. L. Grossiord, and M. C. Poelman, ''Characterization of a sucrose ester microemulsion by freeze fracture electron micrograph and small angle neutron scattering experiments,'' Langmuir **15**, 2307–2315 (1999).

Veenstra, H., B. J. J. van Lent, J. van Dam, and A. P. de Boer, ''Co-continuous morphologies in polymer blends with SEBS block copolymers,'' Polymer **40**, 6661–6672 (1999).

Vigild, M. E., C. Chu, M. Sugiyama, K. A. Chaffin, and F. S. Bates, ''Influence of shear on the alignment of a lamellae-forming pentablock copolymer,'' Macromolecules **34**, 951–964 (2001).

Warr, G. G., ''Shear and elongational rheology of ternary microemulsions,'' Colloids Surf., A **103**, 273–279 (1995).

Washburn, N. R., T. P. Lodge, and F. S. Bates, ''Ternary polymer blends as model surfactant systems,'' J. Phys. Chem. B **104**, 6987–6997 (2000).

Yamamoto, J. and H. Tanaka, ''Shear-induced sponge-to-lamellar transition in a hyperswollen lyotropic system,'' Phys. Rev. Lett. **77**, 4390–4393 (1996).